

# RSC Advances



This is an *Accepted Manuscript*, which has been through the Royal Society of Chemistry peer review process and has been accepted for publication.

*Accepted Manuscripts* are published online shortly after acceptance, before technical editing, formatting and proof reading. Using this free service, authors can make their results available to the community, in citable form, before we publish the edited article. This *Accepted Manuscript* will be replaced by the edited, formatted and paginated article as soon as this is available.

You can find more information about *Accepted Manuscripts* in the [Information for Authors](#).

Please note that technical editing may introduce minor changes to the text and/or graphics, which may alter content. The journal's standard [Terms & Conditions](#) and the [Ethical guidelines](#) still apply. In no event shall the Royal Society of Chemistry be held responsible for any errors or omissions in this *Accepted Manuscript* or any consequences arising from the use of any information it contains.

# **Co-delivery of paclitaxel and indocyanine green by PEGylated graphene oxide: a potential integrated nanoplatform for tumor theranostic†**

Chao Zhang,\* Tan Lu, Jingang Tao, Guang Wan and Hongxing Zhao

*Department of Orthopaedic Surgery, the First Affiliated Hospital of Xinxiang Medical University, Xinxiang 453100, China.*

*\*Corresponding author: Chao Zhang (C. Zhang). E-mail: czhang\_surg@sina.com.*

†Electronic supplementary information (ESI) available.

Herein, we have prepared PEGylated nano graphene oxide (NGO-PEG) that co-delivers the paclitaxel (PTX) and indocyanine green (ICG) for tumor theranostic, integrating fluorescence imaging and chemotherapy. Firstly, polyethylene glycol (PEG) with dual-terminal amine is covalently conjugated with NGO to give the NGO-PEG. And then, ICG, a near-infrared (NIR) fluorescent dye that is approved by Food and Drug Administration (FDA) is covalently loaded onto NGO-PEG as a fluorescence contrast agent, NGO-PEG-ICG. PTX, a widely clinical used anti-cancer drug, is non-covalently immobilized on the NGO surface via  $\pi$ - $\pi$  stacking interaction and hydrogen bonding, giving the multifunctional nano-composite, NGO-PEG-ICG/PTX. The obtained nano-composite has great stability and biocompatibility. NGO-PEG shows (50 $\pm$ 2.1) % and (90 $\pm$ 1.6) % (w/w) of ICG and PTX loading ratios, respectively, which are calculated by UV-vis spectrometer. Fluorescence signal endowed by ICG is detected in the cytoplasm using a confocal microscopy, demonstrating the high-efficiency human osteosarcoma (MG-63) cell uptake of NGO-PEG-ICG/PTX. Moreover, NGO-PEG-ICG/PTX can cause more decrease in cell viability than the same concentration of free PTX, revealing the excellent chemotherapeutic effect of NGO-PEG-ICG/PTX *in vitro*. *In vivo* fluorescence imaging results indicate the high MG-63 tumor accumulation of NGO-PEG-ICG/PTX which can reach the maximum content in tumor about 29.1% dose/g tissue at 24 h post injection and has about eight days of tumor retention. Based on the encouraging results, the NGO-PEG-ICG/PTX is tail vein injected into tumor-bearing mice at day one and day eight, the tumor-bearing mice show complete tumor suppression, no relapse and treatment-induced major organs lesion over one-month treatment. These results suggest that the synthesized versatile NGO-PEG-ICG/PTX with high fluorescence contrast and chemotherapeutic effect can be a potential tumor theranostic nanoplatform.

**Keywords:** paclitaxel, indocyanine green, graphene oxide, fluorescence imaging, tumor theranostic

## Introduction

Recent decades, cancer has already been a serious threat to the human health over the world. Therefore, the tumor precise, clear diagnosis and high-efficiency therapy become more and more important.<sup>1</sup> NIR fluorescence imaging with various NIR contrast agent have been demonstrated extremely high sensitivity and imaging speed for a large field-of-view, which is usually used for clinical diagnosis like identification of tumor margins intraoperatively.<sup>2</sup> Indocyanine green (ICG), a tricarboyanine fluorescence dye, is approved by the FDA for human medical imaging and diagnosis. It exhibits absorption and emission maxima around 740 and 800 nm, respectively. The NIR light (700-1000 nm) has lower light absorptivity by tissue chromophores and tissue scattering.<sup>3,4</sup> Nguyen et al. reviewed that the fluorescence of ICG can guide surgery with live molecular navigation.<sup>5</sup> Van der Vorst et al. had improved sentinel lymph node (SLN) mapping of breast cancer by NIR fluorescence imaging using ICG.<sup>6</sup> However, ICG has several major challenges, such as instability in water, rapid clearance from the body, a short half-life and lack of targeting.<sup>7,8</sup> All these defects limit its utility in NIR biomedical imaging applications.<sup>9,10</sup> Paclitaxel (PTX) is a clinical tumor chemotherapeutic agent, which is approved by the FDA.<sup>11,12</sup> PTX is mostly employed as a treatment drug for ovarian and breast cancer therapy in clinic, and it is also reported that PTX has high toxicity on some other cancers such as non-small-cell lung and prostate cancer.<sup>13-16</sup> However, some serious drawbacks are found on PTX, including low water solubility, poor bioavailability, which will limit its biomedical application.<sup>17</sup> In addition, presently, the dehydrated alcohol with cremophor EL (1:1, v/v) is used as cosolvent for commercialized PTX injection, and further diluted must be done with 0.9% sodium chloride injection prior to use.<sup>18</sup> The cremophor EL is reported that it has serious toxic side effects, such as hypersensitivity reactions and acutely renal function impairment.<sup>19,20</sup> To overcome these limitations of ICG and PTX above, they are usually carried by a multifunctional molecule delivery system.

Graphene oxide (GO), a two-dimensional carbon nanomaterial, has attracted many researchers' interests as its distinct physical and chemical properties such as large surface-to-volume ratio and modifiable surface.<sup>21,22</sup> These merits make them useful in a wide range of applications, especially for drug delivery system. The rich  $\pi$  conjugation structure and oxygen-containing functional groups on nanosized GO (NGO) surface can be modified by some functionalized molecules non-covalently and covalently, respectively.<sup>23-25</sup> However, the NGO has low biocompatibility that will not be beneficial in its biomedical application. Polyethylene glycol (PEG), a surfactant, is often conjugated onto NGO surface (NGO-PEG) to enhance its stability and biocompatibility.<sup>26-28</sup> Recently, Some aromatic anti-tumor drugs like doxorubicin (DOX), SN38 and camptothecin (CPT) are carried by NGO-PEG for tumor chemotherapy, and various fluorescent dyes like fluorescein isothiocyanate (FITC) and rhodamine are loaded onto NGO-PEG surface for fluorescence imaging application.<sup>27,29-32</sup> However, these fluorescent dyes are not approved by FDA and have short fluorescence excitation wavelengths below 700 nm, which have limitation on tissue penetration depth<sup>33-35</sup> Currently, the NGO is used to carry ICG for various medical applications. For example, Chavva et al. have bound ICG conjugated aptamer onto the NGO surface for *in vitro* fluorescence imaging, photothermal and photodynamic treatment,<sup>36</sup> Wang et al. have prepared ICG loaded NGO complex for photothermal therapy and photoacoustic imaging *in vitro*.<sup>37</sup> While, there are seldom reports on *in vivo* fluorescence imaging using ICG based on NGO carrier system.

In this work, we have integrated the ICG and PTX on the NGO-PEG, giving a multifunctional nano-composite, NGO-PEG-ICG/PTX. NIR fluorescence and tumor therapeutic effect are endowed by this nano-composite. The fluorescence property is used to observe the cell uptake of NGO-PEG-ICG/PTX and diagnosis the distribution and tumor retention time in tumor-bearing mice using fluorescence imaging system. Meanwhile, the chemotherapeutic effect of NGO-PEG-ICG/PTX is conducted *in vitro* and *in vivo*.

We believe that the NGO-PEG-ICG/PTX will be the promising multifunctional agent for tumor theranostic application.

## Experimental section

### Materials

Graphene oxide platelet was purchased from Nanjing XF NANO Materials Tech Co., Ltd.; Poly(ethylene glycol) bis (3-aminopropyl) terminated ( $\text{NH}_2\text{-PEG-NH}_2$ ), 1-ethyl-3-(3-dimethylaminopropyl) carbodiimide (EDC), N-hydroxysuccinimide (NHS), and indocyanine green (ICG) were purchased from Sigma-Aldrich (St. Louis, MO, USA); paclitaxel ( $\geq 99\%$ , Aladin) and triethylamine ( $\text{Et}_3\text{N}$ ) were provided by Shanghai Jingchun biotech corporation; Minimum Essential Media (MEM) and phosphate buffer saline (PBS) were bought from Gibco BRL (Grand Island, NY, USA); Cell Counting Kit-8 (CCK-8) was obtained from Dojindo Laboratories (Kumamoto, Japan).

### Synthesis and characterization of NGO-PEG

20 mg GO platelet was dispersed in 10 mL distilled water and then was ultrasonicated in ice-bath for 3 h, followed by adding  $\text{NH}_2\text{-PEG-NH}_2$  (1 mg/mL), EDC (8 mM) and NHS (10 mM), successively, and stirring at room temperature for 2 h. The resulted suspension was purified by centrifuging with a 15 kDa ultracentrifuge tube (Millipore, USA) and dialyzed against distilled water for several days to remove any redundant PEG and other molecules to obtain covalent PEGylated NGO (NGO-PEG) solution, which was stored at  $4^\circ\text{C}$  for further using. The functional group change of NGO before and after PEGylation was detected using Fourier transfer infrared spectrometer (FT-IR, Thermo Fisher Scientific, USA).

### Synthesis and characterization of NGO-PEG-ICG/PTX

The ICG and PTX co-loaded NGO-PEG (NGO-PEG-ICG/PTX) was prepared by two steps. First step: 2 mg/mL ICG was added to NGO-PEG solution (1 mg/mL) and stirred in the presence of  $\text{Et}_3\text{N}$  (35  $\mu\text{g/mL}$ )

over ice for 1 h and 18 h at room temperature according to the literature.<sup>17,38,39</sup> Excess ICG and other reagent were removed by repeatedly filtering through a 15 kDa filter with centrifugation at 5,000 g for 30 min and dialyzing (MW cutoff = 10 kDa) against distilled water for several days to give covalent ICG conjugated NGO-PEG (NGO-PEG-ICG). Second step: Loading of PTX onto NGO-PEG-ICG was carried out by mixing adequate PTX (dissolved in DMSO) and NGO-PEG-ICG suspension with stirring at 4 °C for 6 h. Unbound PTX and free DMSO were removed by repeatedly dialyzing (MW cutoff = 10 kDa) against distilled water for several days to give purified NGO-PEG-ICG/PTX solution. The morphology of NGO-PEG-ICG/PTX was observed by atomic force microscopy (AFM, Agilent Technologies, USA) and Transmission Electron Microscope (TEM, LIBRA 120, ZEISS, Germany). The average particle size and Zeta potential of NGO-PEG-ICG/PTX were determined using a Nanosizer ((Malvern Instruments, UK). The fluorescence-emission of free ICG and NGO-PEG-ICG/PTX were detected by a Luminescence Spectrometer (Perkin-Elmer, USA). The concentration of bound ICG and PTX were measured by UV-vis spectroscopy (Perkin-Elmer, USA) with absorption intensity at 800 nm and 232 nm, respectively. ICG and PTX loading ratios of NGO-PEG were defined as below. All the measurements were performed in triplicate.

$$\text{ICG loading ratio (\%)} = W_{\text{bound ICG}} / W_{\text{NGO-PEG}} \times 100\% \quad (1)$$

$$\text{PTX loading ratio (\%)} = W_{\text{bound PTX}} / W_{\text{NGO-PEG}} \times 100\% \quad (2)$$

#### **Cell culture and *in vitro* cytotoxicity study**

Human MG-63 osteosarcoma cell line obtained from Shanghai Institute of Cell Biology, Chinese Academy of Sciences were cultured in MEM media supplemented with 10% fetal bovine serum (FBS) and 1% penicillin/streptomycin solution in 5% CO<sub>2</sub> at 37 °C.

For *in vitro* cytotoxicity study, MG-63 cells were cultured in 96-well cell culture plates (10<sup>4</sup> cells/well)

for 24 h, and then were treated by NGO-PEG (0-200  $\mu\text{g}/\text{mL}$ ) for 24, 48 and 72h, respectively, free PTX and NGO-PEG-ICG/PTX (0-100  $\mu\text{g}/\text{mL}$  of PTX) for 24h. And then, the old media in each well were replaced by fresh MEM media (contained 10% CCK-8 solution). After 30 min incubation at 37°C, the relative cell viability was assessed by a microplate reader (Tecan, USA) at an absorbance of 450 nm.

#### **Cell uptake of NGO-PEG-ICG/PTX**

For cell uptake assay, MG-63 cells were plated on a 20 mm petri dish with a density of  $5 \times 10^4$  cells/mL, and grown to about 60% confluency. Subsequently, the cells were incubated with free ICG and NGO-PEG-ICG/PTX (30  $\mu\text{g}/\text{mL}$  of ICG) for 2 h in the dark. After washing by PBS for three times, the cells were fixed in 4% paraformaldehyde at 4 °C for 30 min and stained with DAPI (1  $\mu\text{g}/\text{mL}$ ), a DNA-specific fluorescent dye, at 37 °C for 5 min. Images were acquired by a confocal fluorescence microscope (Leica TCS SP5 II, Germany).

#### **Animals and tumor model**

BALB/c nude mice (3-5 weeks old) were obtained from Charles River Laboratories (Shanghai, China), all animal welfare and experimental procedures were carried out in accordance with the Guide for the Care and Use of Laboratory Animals. MG-63 tumor models were generated by subcutaneously injecting approximately  $1 \times 10^6$  cells in 150  $\mu\text{L}$  PBS into the back of nude mice. After tumor size reached approximately 100  $\text{mm}^3$ , the mice were randomly divided into different groups for imaging and therapy experiments. The tumor sizes were measured by caliper and calculated as the Volume = (tumor length)  $\times$  (tumor width)<sup>2</sup>/2.

#### ***In vivo* fluorescence imaging**

The fluorescence signals of free ICG and NGO-PEG-ICG/PTX in tumor tissue were collected using a Maestro *in vivo* fluorescence imaging system (CRi, USA). Images were taken at 0, 0.08, 1, 6, 24, 72, 120,

168 and 192 h post injection using a 735 nm excitation wavelength and the camera was filtered using a 780 nm filter. The fluorescence images of excised major organs including tumor, heart, liver, spleen, lung and kidney at 24h post injection with free ICG and NGO-PEG-ICG/PTX were also collected and analyzed by the fluorescence imaging system. In addition, the content of free ICG and NGO-PEG-ICG/PTX in these excised major tissues was detected. In detail, each tissue sample was dissolved in 900 $\mu$ L of lysis buffer. The concentrations of free ICG and NGO-PEG-ICG/PTX in the tissues were determined by the fluorescence spectrum of each diluted tissue lysates using a fluorescence spectrometer. A various concentrations of free ICG were measured to give a standard calibration curve. Blank tissue samples without injection were measured to determine the tissue auto fluorescence level, which were subtracted from the fluorescence intensities of samples with injection of free ICG and NGO-PEG-ICG/PTX during the concentration calculation. The content of free ICG and NGO-PEG-ICG/PTX was presented as the percentage of injected dose per gram of tissue (% ID/g).

### ***In vivo* tumor therapy**

For *in vivo* tumor therapy, the tumor-bearing mice in different groups (seven mice per group) were injected with saline, NGO-PEG-ICG, NGO-PEG-ICG/PTX (10 mg/kg of GO) and free PTX (9 mg/kg), respectively. The tumor sizes and body weight were measured every three days. The relative tumor volumes were calculated as  $V/V_0$  ( $V_0$  was the tumor volume when the treatment was initiated). Tumor-bearing mice with about one-month treatment after tail vein injection with various samples were sacrificed by CO<sub>2</sub> asphyxiation. Major organs (heart, liver, spleen, lung and kidney) from those mice were collected, stained with hematoxylin and eosin (H&E) and examined by a Microscopic digital camera (OLYMPUS DP27, Japan).

## **Results and discussion**

### Synthesis and characterization of NGO-PEG-ICG/PTX

To make a well dispersed and stable NGO-PEG-ICG/PTX solution for biomedical application, covalent PEGylation of NGO (NGO-PEG) was prepared according the literature.<sup>17,38</sup> Firstly, GO was obtained by oxidization of graphite according to the modified Hummers' method and was ultrasonicated in ice-bath to give the NGO suspension.<sup>40,41</sup> NH<sub>2</sub>-PEG-NH<sub>2</sub> was used to covalently conjugate with NGO by chemical reaction between -NH<sub>2</sub> group of PEG and -COOH group of NGO under the participation of NHS and EDC, resulting in NGO-PEG. PEGylation is often used to promote the biocompatibility of NGO.<sup>42,43</sup> Secondly, ICG was conjugated with NGO-PEG via covalent bond in the presence of Et<sub>3</sub>N to obtain ICG loaded NGO-PEG (NGO-PEG-ICG). Thirdly, PTX was loaded onto the NGO surface by  $\pi$ - $\pi$  stacking interaction, giving the PTX loaded NGO-PEG-ICG (NGO-PEG-ICG/PTX) (Fig. 1A).

The morphology of NGO-PEG-ICG/PTX was visualized by AFM and TEM. As shown in Fig. 1B and the inset, the NGO-PEG-ICG/PTX was flakiness which was in accordance with the TEM image (Fig. S1), and the thickness was about 1–2 nm. The sizes of NGO, NGO-PEG and NGO-PEG-ICG/PTX measured by a Nanosizer (Fig. 1C) showed approximately 70 nm, 76 nm and 95 nm in average size, respectively. Compared with NGO, the average size of NGO-PEG and NGO-PEG-ICG/PTX increased approximately 8 and 25 nm, respectively. These results may indicate the successful PEGylation, ICG and PTX conjugation with NGO. Moreover, the images of NGO, NGO-PEG and NGO-PEG-ICG/PTX solution were showed in Fig. 1D.

The covalent PEGylation of NGO was confirmed by a FT-IR spectrometer. As shown in Fig. 2A, the presence of intense bands at around 2800 cm<sup>-1</sup> (-CH<sub>2</sub>-) and the existence of characteristic amide-carbonyl (-NH-CO-) stretching vibration (~1,650 cm<sup>-1</sup>) definitely illustrated the covalent grafting of PEG chains onto the surface of NGO sheets by amido bond.<sup>44</sup> Fig. 2B showed the UV-vis absorbance

spectra of ICG, NGO-PEG, PTX and NGO-PEG-ICG/PTX. The UV-vis absorbance spectra of NGO-PEG only had a wide absorption peak at 230 nm in the range of 200 to 850 nm. While, after conjugating with ICG and PTX, the spectrum of NGO-PEG-ICG/PTX showed a distinct absorption peak at 232 nm originated from PTX and at around 800 nm originated from ICG, demonstrating the successful binding of PTX and ICG to NGO-PEG. According to the equation (1) and (2), it was calculated that the NGO-PEG had ICG and PTX loading ratios of  $(50 \pm 2.1) \%$  and  $(90 \pm 1.6) \%$  (w/w), respectively. Fig. 2C showed the fluorescence spectrum of the NGO-PEG-ICG/PTX with the maximum emission wavelength at 800 nm which was similar with that of free ICG. Moreover, Fig. S2 showed that there was no severe fluorescence intensity change of the NGO-PEG-ICG/PTX over 14 days at 4 °C, while the fluorescence intensity of free ICG dropped to ~20% of its initial value at the same condition, indicating the great fluorescence stability of NGO-PEG-ICG/PTX.

The PTX release from NGO-PEG at pH 5.0 and 7.4 was investigated to simulate the neutral environment of blood circulation, acidic one in solid tumor tissue and intracellular lysosomes, respectively.<sup>45</sup> As shown in Fig. 2D, the release rate of PTX from NGO-PEG surface at pH 5.0 in PBS was rapidest than that at pH 7.4 and 9.0. It showed that the PTX release had time-dependence, which can be exploited for drug delivery application.

As shown in Fig. 3A and S3, the average size of NGO-PEG and NGO-PEG-ICG/PTX in water almost had no obvious change, as well as the average diameter of NGO-PEG-ICG/PTX in PBS and fetal bovine serum (FBS), while the NGO aggregated from 60 nm to 138 nm over 14 days at 4 °C likely as the result of the  $\pi$ - $\pi$  stacking between NGO surface. In addition, the Zeta potential of NGO-PEG-ICG/PTX detected using a Nanosizer was -28.9 mV (Fig. S4). These results demonstrated that NGO-PEG-ICG/PTX had better stability for long-term storage than that of NGO, which may be due to the PEGylation of NGO.

UV-vis spectrometer was further used to confirm the NGO-PEG-ICG/PTX stability in water. As shown in Fig. 3B and C, a good linear relationship ( $R^2=0.9933$ ) was presented between the concentration of NGO-PEG-ICG/PTX and its absorbance value at 800 nm, indicating the great dispersibility of NGO-PEG-ICG/PTX below 1 mg/mL in water based on the Lambert-Beer's law in homogeneous solution.<sup>46,47</sup> The great stability of NGO-PEG-ICG/PTX will be beneficial in its biomedical application.

#### **Cell uptake and cytotoxicity**

To investigate the cell uptake, NGO-PEG-ICG/PTX as a fluorescent probe was directly incubated with MG-63 cells for 2 h in a 37 °C incubator. And then, the nuclei of MG-63 cell were stained by DAPI. Compared with the free ICG treated group, stronger fluorescence signal of ICG was seen in cytoplasm in NGO-PEG-ICG/PTX group (Fig. 4A), illustrating that NGO-PEG as a carrier could high-efficiency enter cells and locate in cytoplasm.

Next, CCK-8 assay was used to examine the cytotoxicity of NGO-PEG, free PTX and NGO-PEG-ICG/PTX on MG-63 cells. The MG-63 cells exposed in 10, 50, 100, 150 and 200 µg/mL of NGO-PEG for 24, 48 and 72 h, respectively, showed no significant decrease of cell viability (Fig. 4B), indicating that our as-synthesized nanocarrier had low cytotoxicity and good biocompatibility. As shown in Fig. 4C, PTX had dose-dependent (0-100 µg/mL) cell inhibition effect on MG-63 cells. Free ICG below 100 µg/mL almost had no cytotoxicity to MG-63 cells (Fig. S5). However, NGO-PEG-ICG/PTX with the same dose of PTX exhibited more significant cytotoxicity on MG-63 cells than free PTX (Fig. 4C,  $p<0.05$ ). Supposedly, NGO-PEG as nanocarrier with good biocompatibility and appropriate size could more easily entered cells to deliver effective amount of drugs to perform a noticeable therapeutic effect.

#### ***In vivo* fluorescence imaging**

The accumulation profile of free ICG and NGO-PEG-ICG/PTX in MG-63 tumor-bearing mice was measured by *in vivo* fluorescence imaging system. As shown in Fig. 5A, the fluorescence signals distributed extensively in liver tissue and less in tumor after 5 min post injection, and completely disappeared after 24 h post injection for free ICG treated mice. On the contrary, the fluorescence signals of NGO-PEG-ICG/PTX in tumor strengthened with the increase of blood circulation time, which can clearly identify the tumor location after 1 h post injection and still could be detected at day eight (Fig. 5B). The *ex vivo* fluorescence images of excised organs (tumor, heart, liver, spleen, lung and kidney) demonstrated that most of ICG accumulated in the liver and kidney at 24 h tail vein post injection of free ICG, while the NGO-PEG-ICG/PTX distinctly increased the accumulation in tumor, followed by liver and kidneys (Fig. 5C). As shown in Fig. 5D, at 24 h post injection, the content of NGO-PEG-ICG/PTX in tumor reached maximum of about 29.1% dose/g tissue, while the free ICG content in tumor was only 2.03% dose/g tissue, suggesting high tumor accumulation ratio of NGO-PEG-ICG/PTX. According to these results, the NGO-PEG can be used as a great carrier to deliver anti-cancer drug for tumor chemotherapy.<sup>48-50</sup>

### ***In vivo* chemotherapy**

For *in vivo* chemotherapy, tumor-bearing mice were randomly divided into four groups (seven mice per group). Base on the encouraging results that the high-efficiency tumor accumulation of NGO-PEG-ICG/PTX. 100  $\mu$ L saline (Control), free PTX (9 mg/kg), NGO-PEG-ICG and NGO-PEG-ICG/PTX with the same dose of GO (10 mg/kg) were tail vein injected into the tumor-bearing mice in four groups twice (at day one and day eight), respectively. As depicted in Fig. 6A, there were no intense inhibition effects on tumor growth for Control, NGO-PEG-ICG and free PTX treated mice. Significantly, NGO-PEG-ICG/PTX treated mice showed complete suppression in tumor growth and had

no tumor relapse over about one-month treatment. As comparison, there was distinct tumor recurrence detected from day nine for once NGO-PEG-ICG/PTX injected mice at day one (Fig. S6). All these treated mice didn't had significant weight loss during the treatment (Fig. 6B). In addition, the representative H&E staining images in all groups also showed no obvious lesion of major organs (Fig. 6C), demonstrating that NGO-PEG-ICG, free PTX and NGO-PEG-ICG/PTX had no overt systemic toxicity to mice.

## Conclusions

In summary, the present study has reported the fabrication of versatile theranostic nanoplatform that co-delivers ICG and PTX by NGO-PEG for tumor fluorescence imaging and chemotherapy. The obtained NGO-PEG with good biocompatibility and physiological stability can promote the water solubility of PTX and ICG. *In vitro* fluorescence observation indicates that NGO-PEG-ICG/PTX can largely enter cells. NGO-PEG-ICG/PTX shows more significant inhibition effect on the cells than the same concentration of PTX. *In vivo* fluorescence imaging results show that NGO-PEG-ICG/PTX can highly accumulate in tumor region and sustain for eight days. According to the fluorescence imaging results, the mice with twice tail vein injection of NGO-PEG-ICG/PTX exhibit completely suppression on tumor growth and no noticeable lesion on major organs over one-month treatment. The prepared multifunctional NGO-PEG-ICG/PTX will be a promising tumor theranostic agent for clinical application.

## Acknowledgment

The authors appreciate the professional operation guidance for AFM from Agilent Technologies engineers.

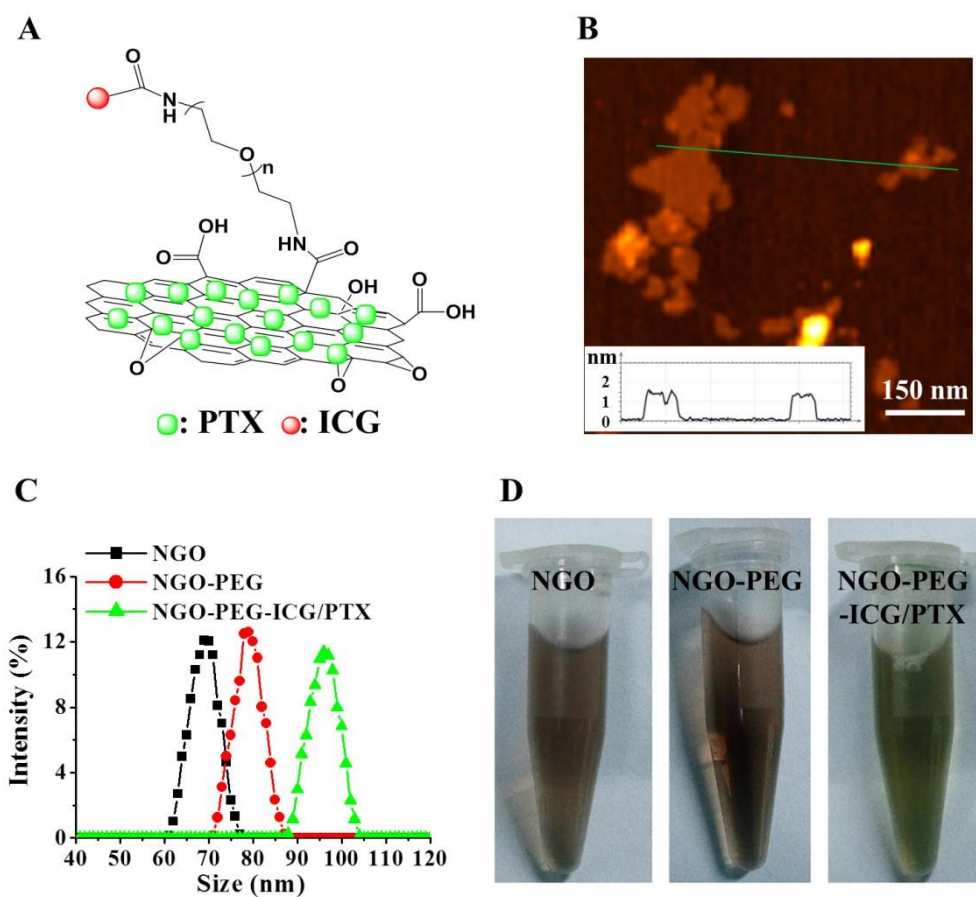
## Notes and references

- 1 B. Sumer and J. Gao, *Nanomedicine*, 2008, **3**, 137-140.
- 2 S. Gioux, H. S. Choi and J. V. Frangioni, *Mol. Imaging*, 2010, **9**, 237-255.
- 3 A. G. Podoleanu, G. M. Dobre, R. Cernat, J. A. Rogers, J. Pedro, R. B. Rosen and P. Garcia, *J. Biomed. Opt.*, 2007, **12**, 115-124.
- 4 Z. Sheng, D. Hu, M. Zheng, P. Zhao, H. Liu, D. Gao, P. Gong, G. Gao, P. Zhang, Y. Ma and L. Cai, *ACS nano*, 2014, **8**, 12310-12322.
- 5 Q. T. Nguyen and R. Y. Tsien, *Nat. Rev. Cancer*, 2013, **13**, 653-662.
- 6 J. R. van der Vorst, B. E. Schaafsma, F. P. Verbeek, M. Hutteman, J. S. Mieog, C. W. Lowik, G. J. Liefers, J. V. Frangioni, C. J. van de Velde and A. L. Vahrmeijer, *Ann. Surg. Oncol.*, 2012, **19**, 4104–4111.
- 7 M. L. Landsman, G. Kwant, G. A. Mook and W. G. Zijlstra, *J. Appl. Physiol.*, 1976, **40**, 575-583.
- 8 A. K. Kirchherr, A. Briel and K. Mäder, *Mol. Pharm.*, 2009, **6**, 480-491.
- 9 Y. Ma, S. Tong, G. Bao, C. Gao and Z. Dai, *Biomaterials*, 2013, **34**, 7706–7714.
- 10 T. K. Hill, A. Abdulahad, S. S. Kelkar, F. C. Marini, T. E. Long, J. M. Provenzale and A. M. Mohs, *Bioconjug. Chem.*, 2015, **26**, 294-303.
- 11 Z. Lu, T. K. Yeh, M. Tsai, J. L. Au and M. G. Wientjes, *Clin. Cancer Res.*, 2004, **10**, 7677-7684.
- 12 X. Y. Yang, Y. X. Li, M. Li, L. Zhang, L. X. Feng and N. Zhang, *Cancer Lett.*, 2012, **334**, 338-345.
- 13 R. A. Karmali, Y. Maxuitenko and G. Gorman, *J. Cancer Ther.*, 2013, **4**, 857-871.
- 14 K. Miller, M. Wang, J. Gralow, M. Dickler, M. Cobleigh, E. A. Perez, T. Shenkier, D. Cella and N. E. Davidson, *N. Engl. J. Med.*, 2007, **357**, 2666-2676.

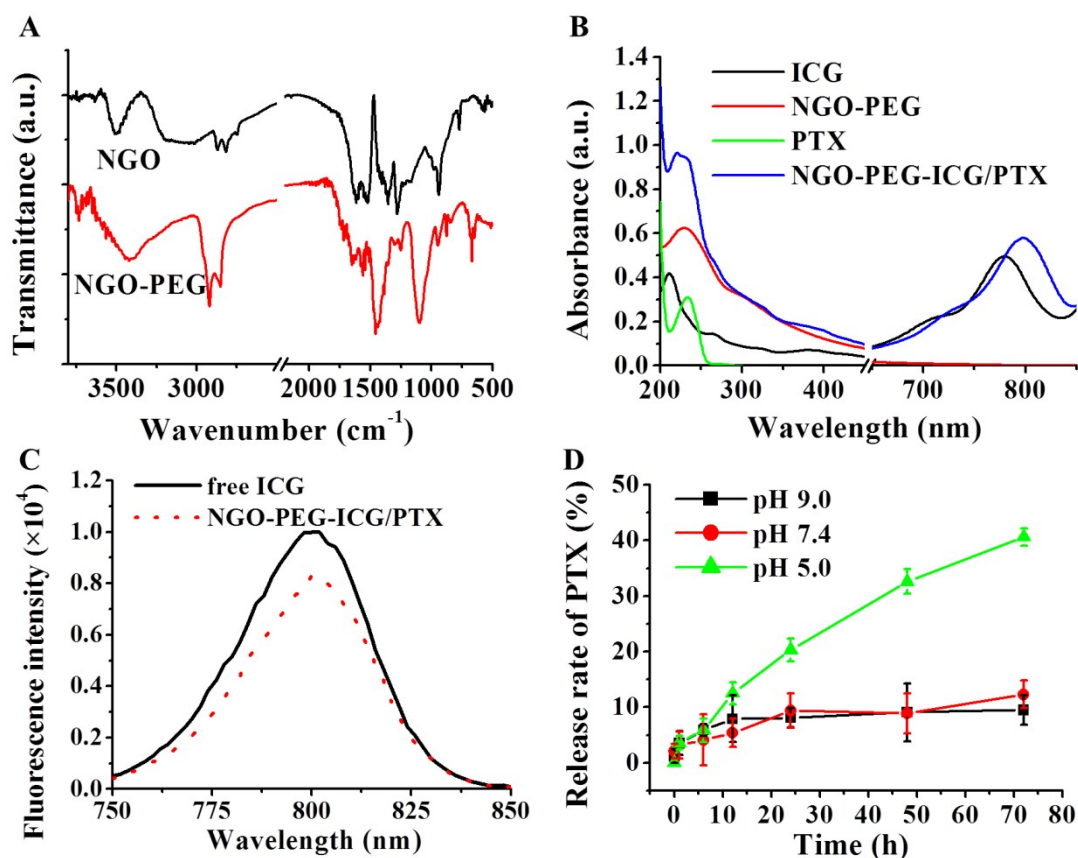
- 15 A. Sandler, R. Gray, M. C. Perry, J. Brahmmer, J. H. Schiller, A. Dowlati, R. Lilenbaum and D. H. Johnson, *N. Engl. J. Med.*, 2006, **355**, 2542-2550.
- 16 M. Hu, J. Zhu and L. Qiu, *RSC Advances*, 2014, **4**, 64151-64161.
- 17 Z. Xu, S. Zhu, M. Wang, Y. Li, P. Shi and X. Huang, *ACS Appl. Mater. Interfaces*, 2015, **7**, 1355-1363.
- 18 Y. Wang, K. C. Wu, B. X. Zhao, X. Zhao, X. Wang, S. Chen, S. F. Nie, W. S. Pan, X. Zhang and Q. Zhang, *Biomed. Res. Int.*, 2011, **2011**, 71-81.
- 19 U. S. Gogate, P. A. Schwartz and S. N. Agharkar, *Pharm. Dev. Technol.*, 2009, **14**, 1-8.
- 20 S. C. Kim, D. W. Kim, Y. H. Shim, J. S. Bang, H. S. Oh, S. Wan Kim and M. H. Seo, *J. Control Release*, 2001, **72**, 191-202.
- 21 F. Perrozzi, S. Prezioso and L. Ottaviano, *J. Phys. Condens. Matter.*, 2014, **27**, 013002-013002.
- 22 A. K. Geim and K. S. Novoselov, *Nat. Mater.*, 2007, **6**, 183-191.
- 23 Y. Bian, Z. Y. Bian, J. X. Zhang, A. Z. Ding, S. L. Liu and H. Wang, *Appl. Surf. Sci.*, 2015, **329**, 269–275.
- 24 V. Georgakilas, M. Otyepka, A. B. Bourlinos, V. Chandra, N. Kim, K. C. Kemp, P. Hobza, R. Zboril and K. S. Kim, *Chem. Rev.*, 2012, **112**, 6156-6214.
- 25 J. Liu, C. Liang and D. Losic, *Acta Biomater.*, 2013, **9**, 9243–9257.
- 26 H. Bao, Y. Pan, Y. Ping, N. G. Sahoo, T. Wu, L. Li, J. Li and L. H. Gan, *Small*, 2011, **7**, 1569-1578.
- 27 Z. Liu, J. T. Robinson, X. Sun and H. Dai, *J. Am. Chem. Soc.*, 2008, **130**, 10876-10877.
- 28 H. Wang, W. Gu, N. Xiao, L. Ye and Q. Xu, *Int. J. Nanomedicine*, 2014, **9**, 1433-1442.
- 29 J. Chen, X. Wang and T. Chen, *Nanoscale Res. Lett.*, 2014, **9**, 1-10.

- 30 G. Gonçalves, M. Vila, M. T. Portolés, M. Vallet-Regí, J. Gracio and P. A. Marques, *Adv. Healthc. Mater.*, 2013, **2**, 1072–1090.
- 31 T. Zhou, X. Zhou and D. Xing, *Biomaterials*, 2014, **35**, 4185–4194.
- 32 Z. Liu, S. Chen, B. Liu, J. Wu, Y. Zhou, L. He, J. Ding and J. Liu, *Anal. Chem.*, 2014, **86**, 12229-12235.
- 33 Z. Xu, S. Wang, Y. Li, M. Wang, P. Shi and X. Huang, *ACS Appl. Mater. Interfaces*, 2014, **6**, 17268-17276.
- 34 R. Zhang, M. Hummelgård, G. Lv and H. Olin, *Carbon*, 2011, **49**, 1126-1132.
- 35 S. A. Hilderbrand and R. Weissleder, *Curr. Opin. Chem. Biol.*, 2010, **14**, 71-79.
- 36 S. R. Chavv, A. Pramanik, B. P. V. Nellore, S. S. Sinha, B. Yust, R. Kanchanapally, Z. Fan, R. A. Crouch, A. K. Singh, B. Neyland, K. Robinson, X. M. Dai, D. Sardar, Y. F. Lu and P. C. Ray, *Part. Part. Syst. Char.*, 2014, **31**, 1252-1259.
- 37 Y. W. Wang, Y. Y. Fu, Q. Peng, S. S. Guo, G. Liu, J. Li, H. H. Yang and G. N. Chen, *J. Mater. Chem. B*, 2013, **1**, 5762-5767.
- 38 Z. Hu, J. Li, Y. D. Huang, L. Chen and Z. H. Li, *RSC Advances*, 2015, **5**, 654-664.
- 39 A. J. L. Villaraza, D. E. Milenic and M. W. Brechbiel, *Bioconjug. Chem.*, 2010, **21**, 2305-2312.
- 40 W. S. Hummers and R. E. Offeman, *J. Am. Chem. Soc.*, 1958, **80**.
- 41 D. A. Dikin, S. Stankovich, E. J. Zimney, R. D. Piner, G. H. Dommett, G. Evmenenko, S. T. Nguyen and R. S. Ruoff, *Nature*, 2007, **448**, 457-460.
- 42 L. Cui, C. Tang and C. Yin, *Carbohydr. Polym.*, 2012, **87**, 2505-2511.
- 43 H. Wen, C. Dong, H. Dong, A. Shen, W. Xia, X. Cai, Y. Song, X. Li, Y. Li and D. Shi, *Small*, 2012, **8**, 760–769.

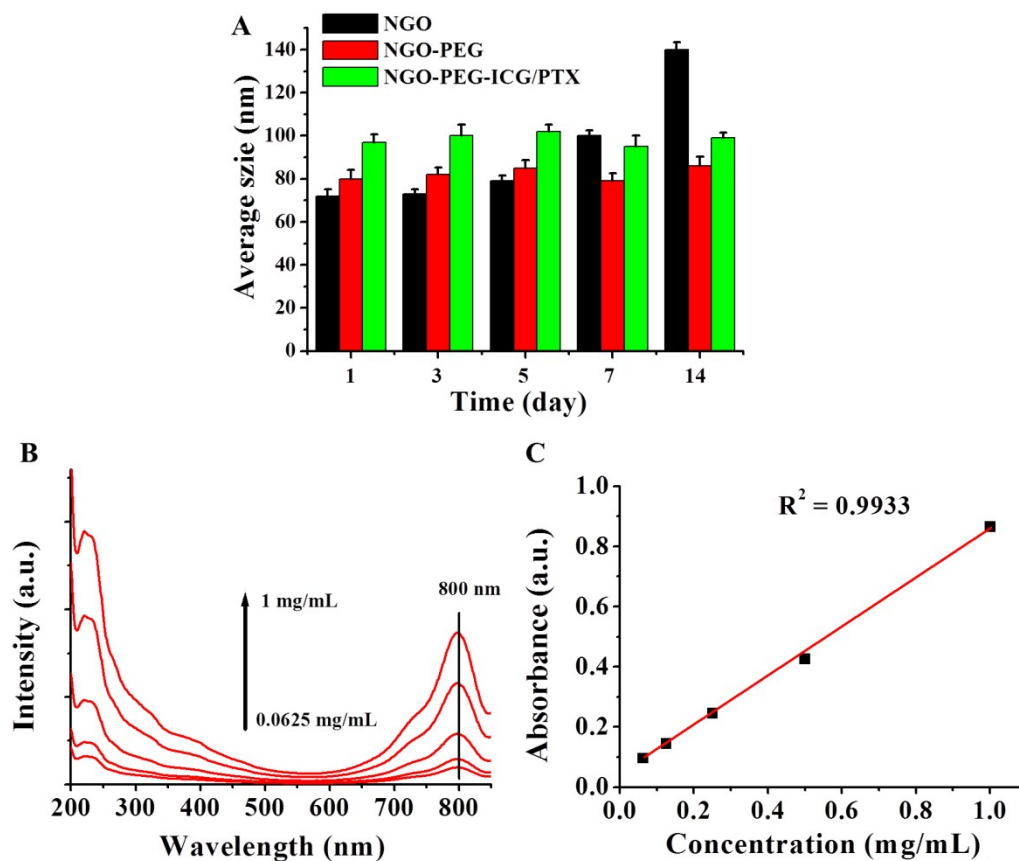
- 44 L. M. Zhang, Z. L. Wang, Z. X. Lu, H. Shen, J. Huang, Q. H. Zhao, M. Liu, N. Y. He and Z. J. Zhang, *J. Mater. Chem. B*, 2013, **1**, 749-755.
- 45 J. M. Li, Y. Y. Wang, W. Zhang, H. Su, L. N. Ji and Z. W. Mao, *Int. J. Nanomedicine*, 2013, **8**, 2101-2117.
- 46 L. Yan, P. R. Chang, P. Zheng and X. Ma, *Carbohydr. Polym.*, 2012, **87**, 1919–1924.
- 47 Q. Yang, X. Pan, F. Huang and K. Li, *J. Phys. Chem. C*, 2010, **114**, 3811-3816.
- 48 U. Prabhakar, H. Maeda, R. K. Jain, E. M. Sevick-Muraca, W. Zamboni, O. C. Farokhzad, S. T. Barry, A. Gabizon, P. Grodzinski and D. C. Blakey, *Cancer Res.*, 2013, **73**, 2412-2417.
- 49 A. P. Subramanian, S. K. Jaganathan and E. Supriyanto, *RSC Advances*, 2015, **5**, 72638-72652.
- 50 S. Shen, F. Kong, X. Guo, L. Wu, H. Shen, M. Xie, X. Wang, Y. Jin and Y. Ge, *Nanoscale*, 2013, **5**, 8056-8066.



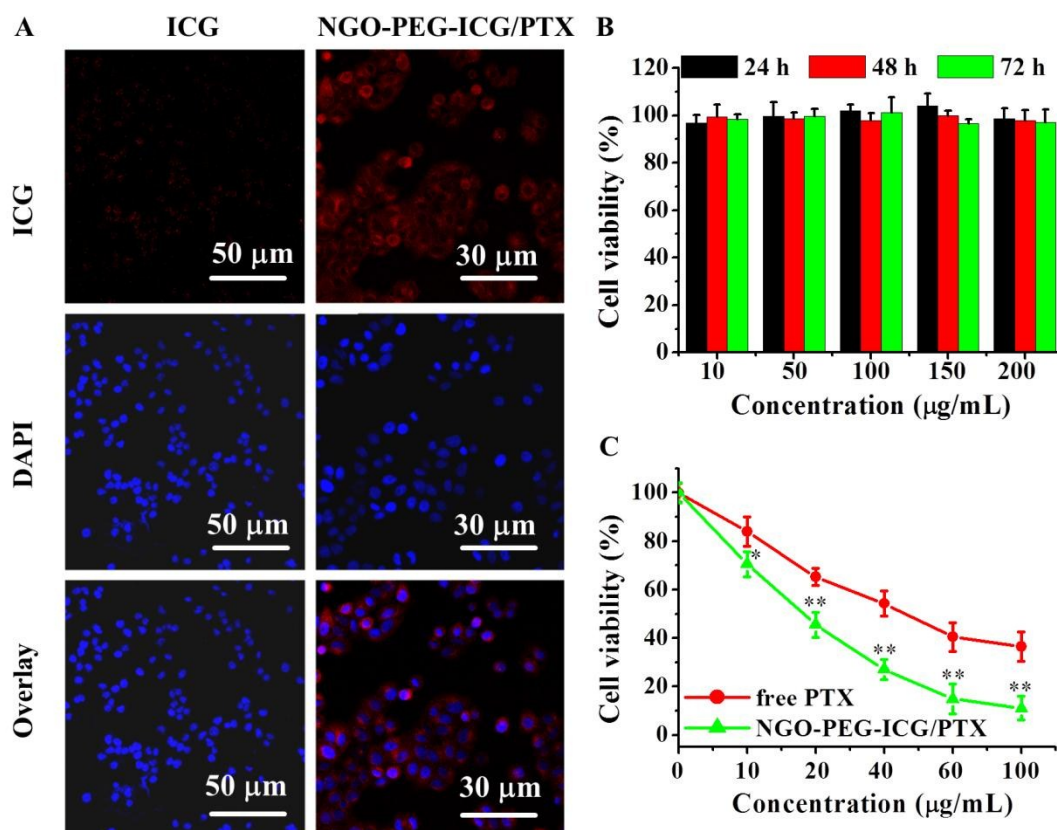
**Fig. 1** (A) The scheme of NGO-PEG-ICG/PTX. (B) The AFM image of NGO-PEG-ICG/PTX. (C) The size distribution of NGO, NGO-PEG and NGO-PEG-ICG/PTX. (D) The photos of NGO, NGO-PEG and NGO-PEG-ICG/PTX water solutions.



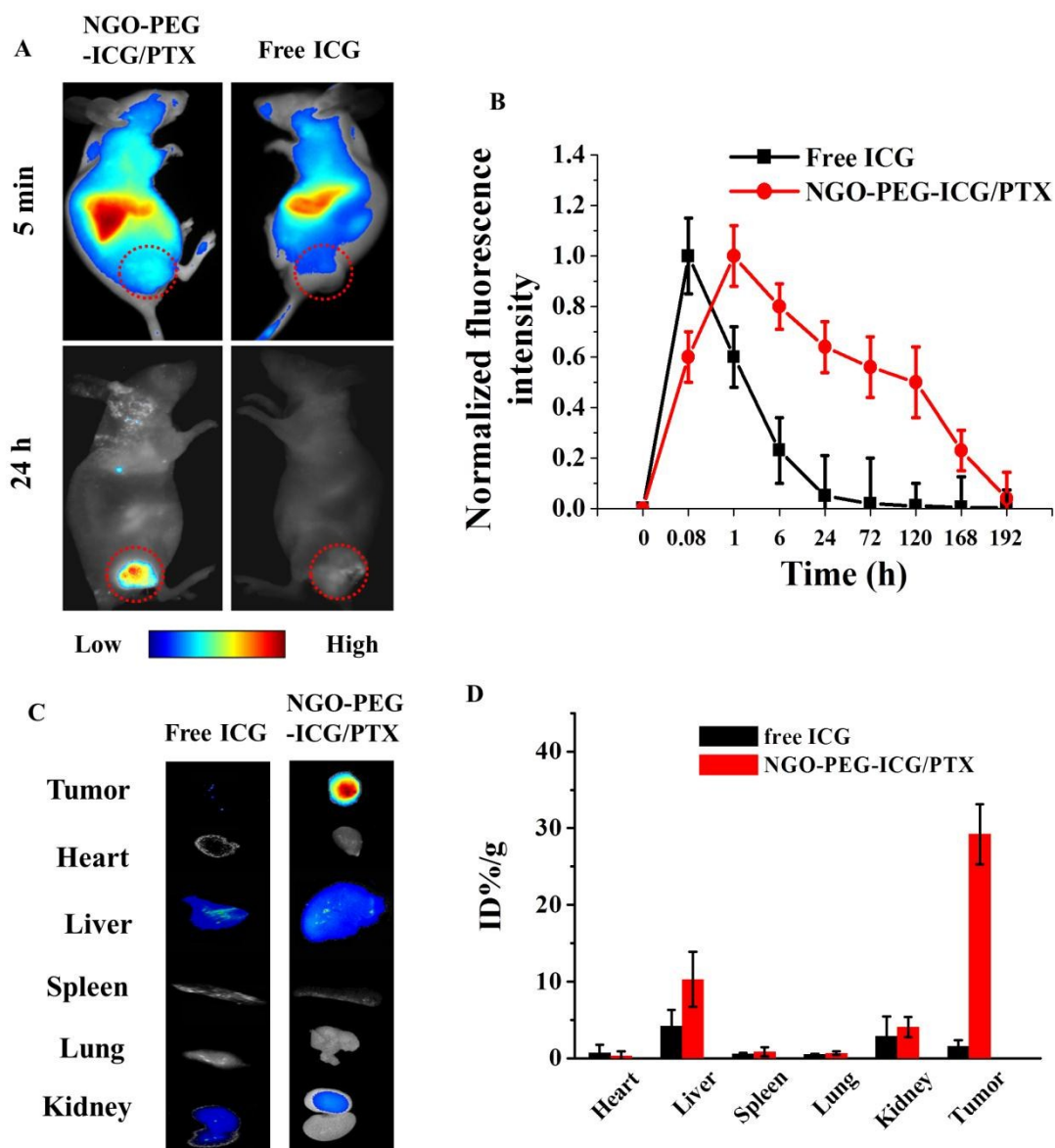
**Fig. 2** (A) The FT-IR spectra of NGO and NGO-PEG. (B) The absorbance spectra of PTX in DMSO ( $50\mu\text{g/mL}$ ), ICG ( $50\mu\text{g/mL}$ ), NGO-PEG ( $50\mu\text{g/mL}$ ) and NGO-PEG-ICG/PTX ( $0.2\text{ mg/mL}$ ) in water. Path length = 1 cm. (C) The fluorescence spectra of ICG and NGO-PEG-ICG/PTX water solution at the same concentration of ICG ( $40\mu\text{g/mL}$ ). Path length = 1 cm. (D) The PTX release on the NGO-PEG-ICG/PTX under the various pH values. The data are shown as mean  $\pm$ SD ( $n = 3$ ).



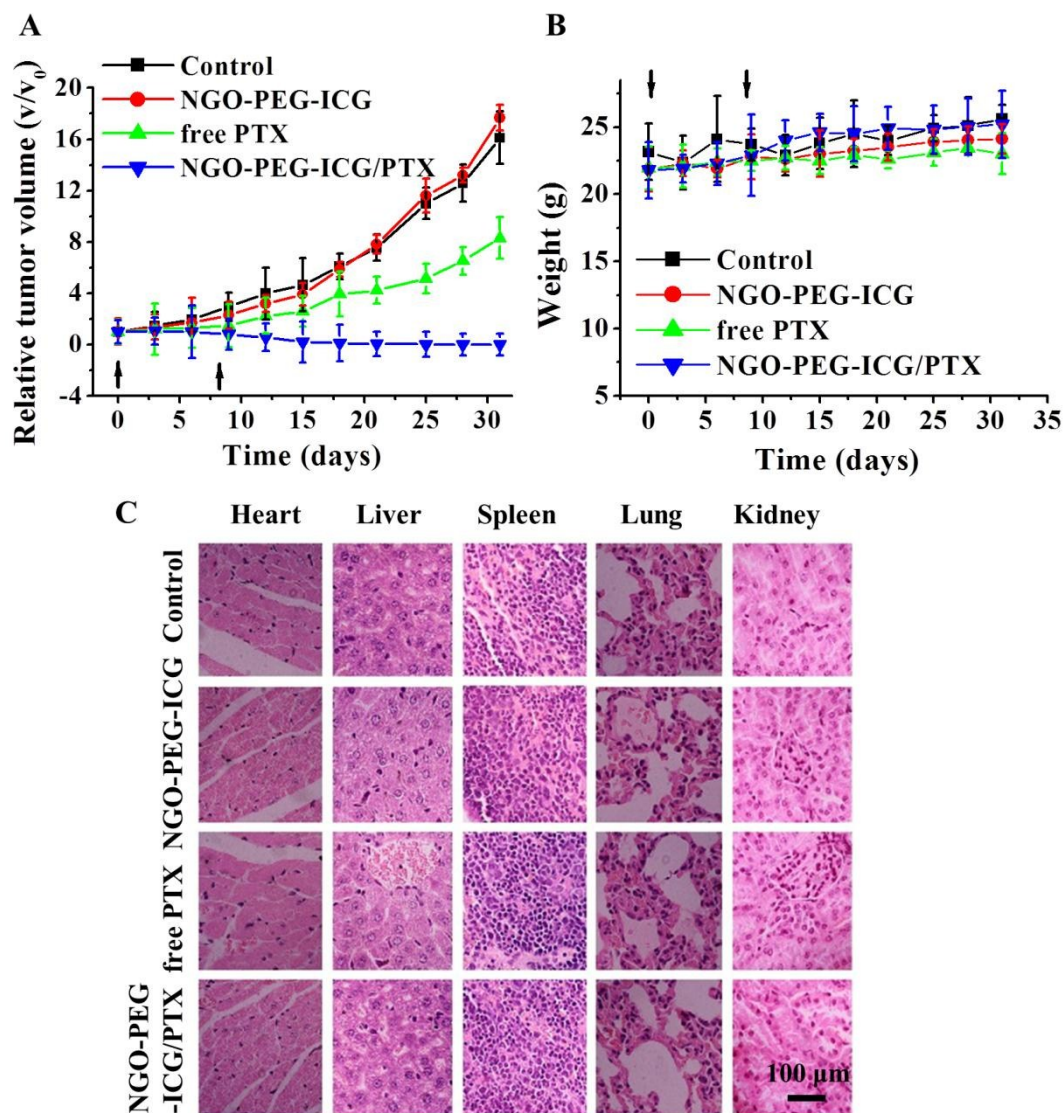
**Fig. 3** (A) The average sizes of NGO, NGO-PEG and NGO-PEG-ICG/PTX over 14 days at 4°C. The data are shown as mean  $\pm$  SD ( $n = 3$ ). (B) UV-vis absorbance spectra of NGO-PEG-ICG/PTX water solution in various concentrations (0.0625, 0.125, 0.25, 0.5 and 1 mg/mL). Path length = 1 cm. (C) The correlation between the NGO-PEG-ICG/PTX absorbance value at 800 nm and its concentration.



**Fig. 4** (A) The cell uptake of free ICG and NGO-PEG-ICG/PTX. (B) The cytotoxicity of different concentrations of NGO-PEG on MG-63 cells at various treating time. (C) The cytotoxicity of different concentrations of free PTX and NGO-PEG-ICG/PTX (at the same concentration of PTX) on MG-63 cells. The data are shown as mean  $\pm$  SD ( $n = 3$ ). \* $p < 0.05$ , \*\* $p < 0.01$ , compared with the free PTX group at the same concentration.

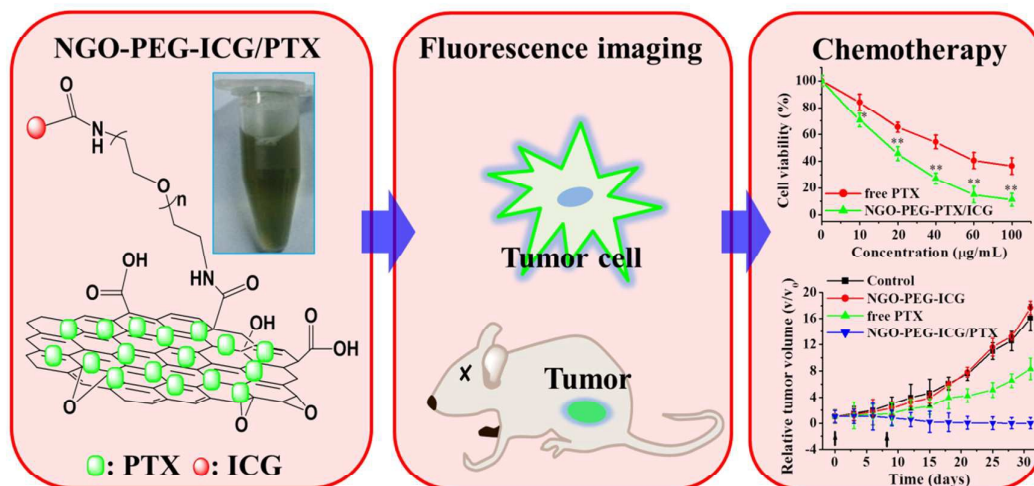


**Fig. 5** (A) The representative fluorescence images of tumor-bearing mice after tail vein injection with free ICG and NGO-PEG-ICG/PTX. The red dashed circles indicated the tumor region. (B) Quantitative analysis of *in vivo* fluorescence signal of tumor regions as injection time. (C) *Ex vivo* fluorescence images of tumors and major organs at 24 h post injection of free ICG and NGO-PEG-ICG/PTX. (D) Biodistribution of free ICG and NGO-PEG-ICG/PTX in mice determined by the ICG fluorescence from diluted tissue lysates.



**Fig. 6** (A) The relative tumor volume and (B) body weight of tumor-bearing mice after tail vein injection with saline (Control), NGO-PEG-ICG, PTX and NGO-PEG-ICG/PTX, respectively. Black arrows indicated injection time point. (C) The representative H&E staining images of major organs of tumor-bearing mice after one-month treatment.

## Graphic Abstract



The schematic of the present NGO-PEG-ICG/PTX for tumor theranostic, integrating fluorescence imaging and chemotherapy.